

**UCC Library and UCC researchers have made this item openly available.  
Please [let us know](#) how this has helped you. Thanks!**

<b>Title</b>	Synchronization in functional networks of the human brain
<b>Author(s)</b>	Hövel, Philipp; Viol, Aline; Loske, Philipp; Merfort, Leon; Vuksanović, Vesna
<b>Publication date</b>	2018-10-25
<b>Original citation</b>	Hövel, P., Viol, A., Loske, P., Merfort, L. and Vuksanović, V. (2018) 'Synchronization in Functional Networks of the Human Brain', Journal of Nonlinear Science, doi: 10.1007/s00332-018-9505-7
<b>Type of publication</b>	Article (peer-reviewed)
<b>Link to publisher's version</b>	<a href="https://link.springer.com/article/10.1007%2Fs00332-018-9505-7">https://link.springer.com/article/10.1007%2Fs00332-018-9505-7</a> <a href="http://dx.doi.org/10.1007/s00332-018-9505-7">http://dx.doi.org/10.1007/s00332-018-9505-7</a> Access to the full text of the published version may require a subscription.
<b>Rights</b>	© Springer Science+Business Media, LLC, part of Springer Nature 2018. This is a post-peer-review, pre-copyedit version of an article published in Journal of Nonlinear Science. The final authenticated version is available online at: <a href="http://dx.doi.org/10.1007/s00332-018-9505-7">http://dx.doi.org/10.1007/s00332-018-9505-7</a>
<b>Embargo information</b>	Access to this article is restricted until 12 months after publication by request of the publisher
<b>Embargo lift date</b>	2019-10-25
<b>Item downloaded from</b>	<a href="http://hdl.handle.net/10468/7138">http://hdl.handle.net/10468/7138</a>

Downloaded on 2019-12-02T14:25:13Z

1 **Synchronization in functional networks of the human**  
2 **brain**

3 **Philipp Hövel\*** · **Aline Viol** · **Philipp**

4 **Loske** · **Leon Merfort** · **Vesna Vuksanović\***

5

6 Received: date / Accepted: date

7 **Abstract** Understanding the relationship between structural and functional or-  
8 ganization represents one of the most important challenges in neuroscience. An  
9 increasing amount of studies show that this organization can be better under-  
10 stood by considering the brain as an interactive complex network. This approach  
11 has inspired a large number of computational models that combine experimental

---

Philipp Hövel

School of Mathematical Sciences, University College Cork, Cork T12 XF62, Ireland  
Institute of Theoretical Physics, Technische Universität Berlin, Hardenbergstraße 36, 10623  
Berlin, Germany

Bernstein Center for Computational Neuroscience Berlin, Humboldt-Universität zu Berlin,  
Philippstraße 13, 10115 Berlin, Germany

E-mail: phoewel@physik.tu-berlin.de

Aline Viol

Institute of Theoretical Physics, Technische Universität Berlin, Hardenbergstraße 36, 10623  
Berlin, Germany

Bernstein Center for Computational Neuroscience Berlin, Humboldt-Universität zu Berlin,  
Philippstraße 13, 10115 Berlin, Germany

E-mail: aline.viol@bccn-berlin.de

Philipp Loske

Institute of Theoretical Physics, Technische Universität Berlin, Hardenbergstraße 36, 10623  
Berlin, Germany

Leon Merfort

Institute of Theoretical Physics, Technische Universität Berlin, Hardenbergstraße 36, 10623  
Berlin, Germany

Vesna Vuksanović

Aberdeen Biomedical Imaging Centre, University of Aberdeen, Lilan Sutton Building, Forester-  
hill, Aberdeen AB25 2ZD, UK

E-mail: vesna.vuksanovic@abdn.ac.uk

\*These authors contributed equally.

12 data with numerical simulations of brain interactions. In this paper, we present a  
13 summary of a data-driven computational model of synchronization between distant  
14 cortical areas that share a large number of overlapping neighboring (anatomical)  
15 connections. Such connections are derived from in-vivo measures of brain connec-  
16 tivity using diffusion-weighted magnetic resonance imaging and are additionally  
17 informed by the presence of significant resting-state functionally correlated links  
18 between the areas involved. The dynamical processes of brain regions are simu-  
19 lated by a combination of coupled oscillator systems and a hemodynamic response  
20 model. The coupled oscillatory systems are represented by the Kuramoto phase os-  
21 cillators, thus modeling phase synchrony between regional activities. The focus of  
22 this modeling approach is to characterize topological properties of functional brain  
23 correlation related to synchronization of the regional neural activity. The proposed  
24 model is able to reproduce remote synchronization between brain regions reaching  
25 reasonable agreement with the experimental functional connectivities. We show  
26 that the best agreement between model and experimental data is reached for dy-  
27 namical states that exhibit a balance of synchrony and variations in synchrony  
28 providing the integration of activity between distant brain regions.

## 29 **1 Introduction**

30 Decoding the fundamental mechanisms underlying large-scale brain integration is  
31 one of the major challenges of neuroscience. A dominant hypothesis states that  
32 phase synchronization plays an important role for the integration of the neural  
33 activities between distant sites of the brain. The interaction among distributed  
34 brain regions through phase synchronization may form the basis for cognitive

35 processing [1–3]. An increasing number of literature aims to establish a framework  
36 of models designed to deal with this issue by means of shaping patterns of the  
37 large-scale functional connectivity map [4–8].

38 In this paper, we discuss neural synchronization using simple concepts of oscil-  
39 lators’ dynamics [9]. To this purpose, we review a data-driven approach that uses  
40 a network of Kuramoto models to simulate phase synchrony in the brain at rest  
41 [10–12]. This is one of the models that aim to recover the interplay between brain  
42 structural and functional connectivity from the perspective of coupled oscillatory  
43 processes [13–16]. This model shows that remote synchronization observed in the  
44 brain at rest may be sustained by the shape of structural connectivity and simple  
45 dynamical rules.

46 There is evidence that brain integrative functions cannot be fully predicted  
47 from the anatomical structure [4, 7]. Subsequently, one can argue that the dynam-  
48 ics of information on top of structural connections enables the communication  
49 between segregated brain areas. Kuramoto phase oscillator models have been used  
50 to explore fundamental mechanisms underlying the nature of this communication.  
51 The basic idea is to incorporate topological properties of the large-scale brain  
52 connectivity in the coupling structure of the model. These properties are usu-  
53 ally derived from white-matter tractography. The model that we here present also  
54 takes into account the functional connectivity map and transmission delays based  
55 on realistic distances to help to focus on connections relevant for the brain state  
56 under consideration.

57 Within this framework, dynamical models of the resting brain based on the  
58 Kuramoto phase oscillators have been able to shed light on how (i) the resting-  
59 state brain activity emerges from a sufficient degree of noise and time delays [13,

60 14], (ii) relay-like interactions between distant brain areas emerge from modular  
61 network structures [11], and (iii) the anatomical hubs in the brain synchronize  
62 their activity [17]. A similar approach can be utilized to study pathological states  
63 due to the epilepsy [7], stroke [18] or schizophrenia [19]. An additional common  
64 feature of these models is the presence of variations in network synchrony, which  
65 is indicative of network metastability. This dynamical property allows for flexible  
66 changes of the network synchrony, i.e., partial and time-varying synchronization  
67 of neural activity across regions. These partial synchronization patterns in neural  
68 networks induce fluctuations at the level of synchrony of sub-networks leading to  
69 correlated fluctuations in low-frequency activity present in functional magnetic  
70 resonance imaging (fMRI) time series [13,17,20].

71 This paper is organized as follows: In section 2, we first introduce the con-  
72 cept of brain networks, which can be studied using methods from graph theory.  
73 We then continue by describing principles of nonlinear dynamics principles behind  
74 synchronization models and their application on neural dynamics (section 3). In  
75 section 4, we investigate the role that synchrony and its variations play in brain  
76 activity based on simulated neural/blood-oxygen-level-dependent time series. We  
77 also provide new findings that combine different approaches used in previous stud-  
78 ies. We conclude in section 5 with a brief summary, consider model limitations,  
79 and suggest further studies.

## 80 **2 Brain networks and neuroimaging data**

81 The brain is a complex dynamical system characterized by nonlinear interactions  
82 and emergent behaviors. This description – today nearly a consensus among neu-

83 roscientists – contrasts the approach of brain functional specialization, a concept  
84 widespread until the early 20th century [21]. A common basis of both viewpoints  
85 is the hypothesis that every mental state is connected to a physical brain state.  
86 This hypothesis is known as a *neural correlate* [22]. The functional specialization  
87 approach has triggered considerable contributions to neuroscience. Nevertheless,  
88 it faces serious limitations, mainly when employed to investigate high-level cog-  
89 nitive functions. On the other hand, the complex system approach has been very  
90 promising for such investigations. In short, the focus from the first to the latter  
91 approach has been shifted from where to how cognitive functions take place in the  
92 brain [23].

93 The popularization of the idea of the brain as a complex dynamical system was  
94 especially promoted by the recent development of noninvasive imaging technologies  
95 that were able to record the time-dependent activity in the human brain as a whole  
96 [24]. Among those technologies, functional magnetic resonance imaging (fMRI)  
97 played a particularly important role. Roughly speaking, the data recorded via  
98 those functional neuroimaging techniques consist of temporal series associated  
99 with linear and nonlinear functional relationships between brain regions and are  
100 understood as a proxy for neural activity. These series are recorded from collective  
101 signals of neural populations that form synchronized local circuits. The current  
102 challenge is to unveil the rules behind global brain activity and how they are  
103 connected to the range of cognitive states.

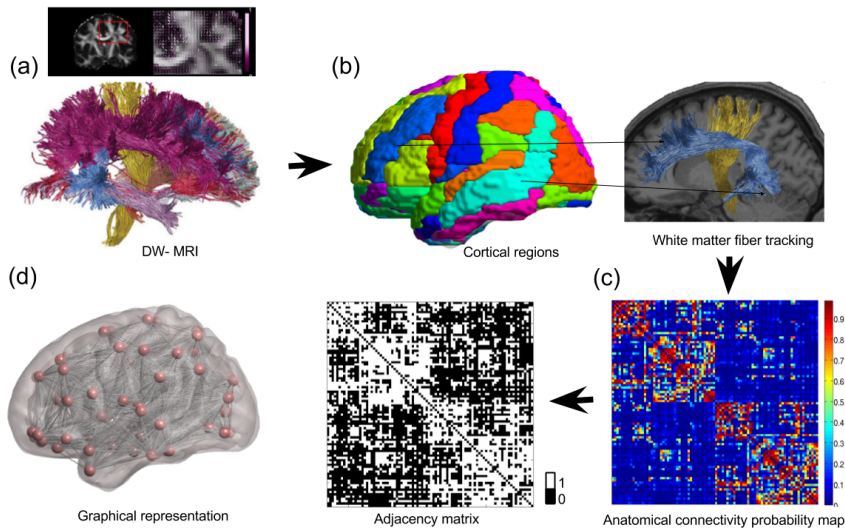


**Fig. 1** Anatomical network. (a) Diffusion-weighted magnetic resonance imaging (DW-MRI) and artistic reconstruction showing the fiber tracts. (b) Parcellation according to a cortical anatomical atlas and density of tracts between two pairs of areas. (c) Matrix of the anatomical connectivity probability of structural connections between pairs of regions. (d) Network construction: adjacency matrix obtained by thresholding and graphical representation of the corresponding structural brain network. Sources: The DW-MRI figure and its artistic reconstruction is a reproduction of reference [25]. The brain images and network were created with the help of BrainNet Viewer [26]. The data for the anatomical connectivity probability is taken from reference [27].

## 104 2.1 Graph theory and brain connectivity maps

105 Graph theory or network science is a novel way to study topology of the structural  
 106 and functional organization of the brain which consists of describing it in terms of  
 107 nodes (brain regions) and edges (the structural connections or functional relation-  
 108 ships). Before we discuss how to define brain connectivity using graph-theoretical  
 109 concepts, it is important to clarify the distinction between two different types of  
 110 large-scale brain connectivity frequently mentioned in the literature.

111 The *anatomical connectivity* map is the map of structural connections between  
 112 brain regions [28]. This network is stable on shorter timescales, but it may change  
 113 over larger times due to neuronal plasticity [23]. The classical way to map struc-  
 114 tural connectivity is tracing neuronal paths by means of invasive and postmortem

115 methods [29]. Due to this fact, it cannot be used to create a large dataset of the hu-  
116 man brain. Alternatives come with the advance of neuroimaging techniques, such  
117 as diffusion-weighted magnetic resonance imaging (DW-MRI), where anatomical  
118 fibers may be inferred by means of statistical models. Such methods allow in-vivo  
119 tractography of white-matter fibers. See references [30–32] for details about struc-  
120 tural connectivity and how to acquire it from the human brain. Figure 1 depicts  
121 a schematic illustration of the workflow to extract a brain graph from imaging  
122 data. In short, the adjacency matrix is obtained from the anatomical connectivity  
123 probability map by thresholding, that is only probabilities above a threshold result  
124 in a link in the brain graph.



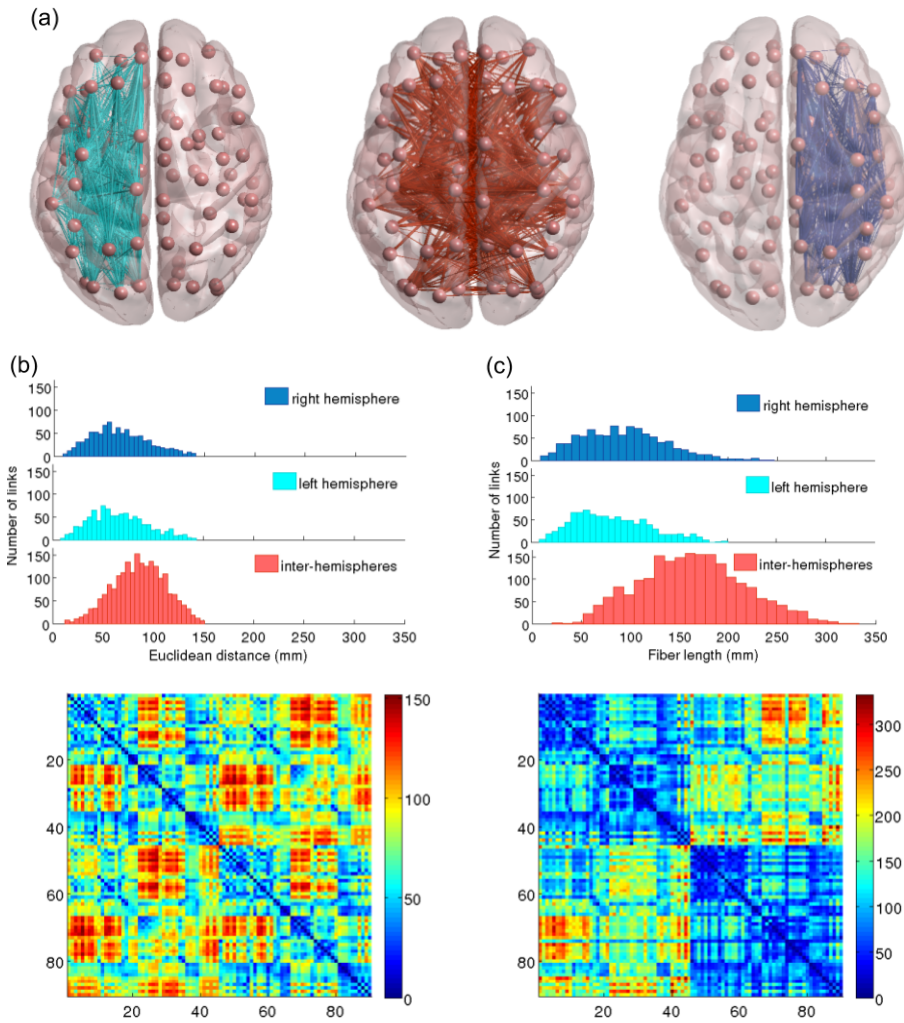


**Fig. 2** Euclidean distances and fiber lengths. (a) Representation of networks, that is 90 brain regions according to the Automated Anatomical Labeling (AAL) parcellation [33] as nodes connected by links in the left hemisphere, between hemispheres, and in the right hemisphere respectively. (b) Top: Histograms of Euclidean distances in the right (blue), left (cyan), and between (red) hemispheres. Bottom: Matrix of the Euclidean distances between pairs of cortical regions. (c) Top: Histograms of the fiber lengths in the right, left, and between hemispheres. Bottom: Matrix of the fiber lengths between pairs of cortical regions. The data of the fiber lengths were taken from reference [27]. The brain networks were created with help of BrainNet Viewer [26].

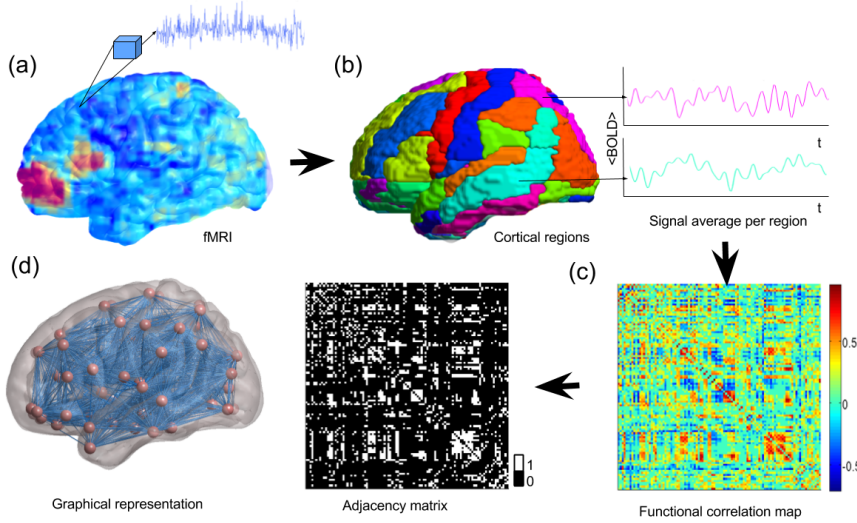


**Fig. 3** Functional network. (a) Functional magnetic resonance imaging (fMRI) and blood-oxygen-level-dependent (BOLD) signals recorded for each voxel. (b) Parcellation according to cortical anatomical atlas and the averages of the signals from two regions. (c) Functional correlation between BOLD time series for every pair of regions. (d) Network construction: the adjacency matrix obtained by thresholding and the corresponding functional brain network. The brain images and network were created with the help of BrainNet Viewer [26].

125 The procedure of DW-MRI leads to an unexpected result. In order to quantify  
 126 the probability, with which two brain regions of interest are structurally con-  
 127 nected, one constructs a three-dimensional trajectory of the fiber tract between  
 128 the centers of those regions. This provides a gateway to measure the length of the  
 129 connection. Figure 2 depicts the distribution and distance matrices of these fiber  
 130 lengths in panel (c). Compared to a naive estimate based on the Euclidean dis-  
 131 tance between regions considered in the Automated Anatomical Labeling (AAL,  
 132 see reference [33]) shown in panel (b), one can see that the distributions of intra-  
 133 and inter-hemispheric connections exhibit qualitatively the same shape and that  
 134 the fiber lengths stretch to larger values. As it will be explained in detail in sec-  
 135 tion 3.2, this distance can be used to approach transmission delays between the  
 136 brain regions.

137 Functional relationships in the brain are usually described in the form of so  
138 called functional connectivity maps. They map the temporal correlations between  
139 regional activities [34], whose modular-like organization supports resting state  
140 networks as well as cognitive and behavioral functions. Therefore, they refer to  
141 a functional relationship irrespective of whether or not there exist anatomical  
142 connections. Functional connectivities are derived from time traces obtained by  
143 recordings of variations in the blood-oxygen-level-dependent signal (BOLD sig-  
144 nal) due to brain activity. For a schematic depiction of the generation of functional  
145 connectivity maps, see figure 3. In this work, we are interested in simulating the  
146 functional connectivity based on networks obtained from neuroimaging data. In  
147 the following, we briefly describe how a functional connectivity map, or functional  
148 network, can be obtained from fMRI data using graph theory.

149 The fMRI data is a 3-dimensional image of the brain acquired over time. At the  
150 finest spatial resolution of such an image, each *voxel* (typically of size 1-2 mm<sup>3</sup>)  
151 gives rise to a single time series. For a large-scale analysis of the whole brain, the  
152 functional network may be defined as follows: The graph nodes represent regions  
153 of interest, usually defined by cortical regions obtained by parcellating the voxels  
154 in the fMRI measurement according to a cortical brain atlas [33,35]. Each of  
155 the resulting regions of interest, that is nodes in the brain network, gives rise  
156 to one time series that represents the BOLD signal in this region. Usually, this  
157 series is obtained by averaging over the respective set of voxels. Subsequently,  
158 network links are defined on the basis of a correlation between time series from  
159 each pair of regions of interest. This method yields a weighted coupled network,  
160 indicating the similarity in the activities of the respective nodes. These maps  
161 *connect* brain regions irrespective of the presence of actual anatomical links. It is

162 worth mentioning that fMRI captures the variation in the BOLD signal, that is,  
163 it is an indirect measurement of neural activity and includes several confounders  
164 [36]. Before constructing functional networks, the data undergoes a number of pre-  
165 processing steps, e.g., for motion correction, to remove spurious information, and  
166 band-pass filtering to improve the signal-to-noise ratio. For further details about  
167 data pre-processing, see references [11,37–39]. For more details about networks  
168 from fMRI data, see references [40–43].

169 One can describe functional networks by an adjacency matrix  $\{A_{ij}\}_{i,j=1,\dots,N}$ ,  
170 in which each matrix element takes the value of unity if a pair of nodes is connected  
171 and zero otherwise. The pair of nodes is considered to be connected when the re-  
172 spective entry in the correlation matrix exceeds a predefined threshold value. There  
173 are different methods used to threshold the matrix and to retain only those values  
174 which are statistically significant. The value of the threshold has a direct influence  
175 on the network density [41]: the higher the threshold, the lower the network den-  
176 sity. By defining its adjacency matrix and thus selecting the network topology, it  
177 is possible to detect universal behaviors of coupled dynamical systems such as syn-  
178 chronization or metastability. One can also consider weighted instead of binarized  
179 matrices. The weight can be added to the model by considering some information  
180 from experimental data. For example, it can be proportional to the density of fiber  
181 tracts between the two cortical regions [44]. In the current approach, however, we  
182 aim for simplicity of the model by considering only anatomically relevant connec-  
183 tions of higher probability. For a detailed overview of complex brain networks, see  
184 reference [45].

---

## 185 2.2 Spontaneous synchronicity and resting state brain networks

186 Most of the early neuroimaging analyses were designed to test the hypothesis of lo-  
187 calized functional brain specificity. The goal was to investigate, which region in the  
188 brain is activated during a specific task. This design is rooted in neuroanatomists'  
189 concepts of the 18th century and was largely discussed at the end of the 20th cen-  
190 tury [21]. In fact, several experiments had supported the paradigm that specific  
191 brain regions are correlated with specific functions, especially basic sensory and  
192 motor tasks [21]. However, the functional specificity started to receive relevant  
193 critical remarks. This reductionist approach could not explain high-level cognitive  
194 processes such as emotions, creativity, and consciousness.

195 In the middle of the 1990's, a new insight changed the focus of research and  
196 transformed prior knowledge. It was recognized that there are large-scale synchro-  
197 nization patterns in the spontaneous fluctuation of brain activities in the absence  
198 of external input [46]. Non-random patterns were observed in the data scanned  
199 from subjects in the resting state, that is lying down in the absence of tasks or at-  
200 tention demands. These findings were corroborated and complemented by several  
201 studies using different neuroimaging techniques [47]. Further descriptions of these  
202 patterns, termed as *resting state networks* (RSN), can be found in references [48,  
203 49]. The discovery of the RSN is considered a milestone in contemporary neuro-  
204 science for different reasons. It supports the regard of the brain as a dynamical  
205 complex system. The detection of large-scale patterns for resting state conditions  
206 reflects the existence of coordinated intrinsic dynamics. This spontaneous inter-  
207 regional synchronization indicates self-organized capability. On one hand, it has  
208 been suggested that RSN are related to high-level brain functions such as inter-

209 nal mental processes and consciousness. This hypothesis is supported by studies  
210 that show variations in statistical features of RSN in altered states of conscious-  
211 ness [50–52] and mental disorders such as autism [53] or schizophrenia [54]. On  
212 the other hand, RSN have also been detected in people subjected to deep seda-  
213 tion [55], sleep [56], coma [57], or even vegetative states [58]. This fact could, in  
214 principle, challenge the hypothesis of RSN as a signature of consciousness. How-  
215 ever, Barttfeld et al. show that RSN in monkey brains under deep anesthesia are  
216 more strongly correlated to the anatomical connectivity map in comparison to  
217 regular RSN in a resting state of wakefulness [59]. They show that in the case  
218 of loss of consciousness, the functional activity is tied to anatomical connectivity.  
219 Their study is in agreement with hypotheses made in previous theoretical works  
220 [5, 60]. Functional networks in resting states where the subject is awake are char-  
221 acterized by long-range synchronicity and high variability of patterns. It had been  
222 observed that an anatomically connected pair of nodes has a high probability to  
223 be functionally connected. However, functional connectivity is frequently observed  
224 between brain regions without direct structural links [5, 61]. The understanding of  
225 the rules that allow both long-range synchronization and flexibility of patterns on  
226 functional networks may be the key to decrypt the mechanisms behind high-level  
227 brain functions. Models using dynamical systems, e.g., oscillator models, are the  
228 most promising tools to tackle this challenge.

### 229 **3 Brain activity and synchronization models**

230 In this section, we build a bridge between nonlinear dynamics and computational  
231 neuroscience. At first, we summarize the concept of synchronization and then

232 develop a simple mathematical model that will be used in section 4. We also  
233 briefly elaborate, how a BOLD signal can be inferred from a neural time series by  
234 means of the Balloon-Windkessel model.

### 235 3.1 Nonlinear dynamics and synchronization in the brain

236 Synchronization plays an important role in various contexts including physics, bi-  
237 ology, and beyond [9, 62–65]. In neuroscience, some forms of cooperative dynamics  
238 have been associated with pathological states like migraine, Parkinson’s disease,  
239 or epilepsy [66–76]. Besides these detrimental forms of synchrony, it is also con-  
240 sidered a crucial mechanism for recognition, learning, and processing of neural  
241 information.

242 In general, neuronal systems can be described by physiological models such  
243 as the Hodgkin-Huxley equations [77]. These type of models account for many  
244 physiological details and processes. Accordingly, they offer a detailed description  
245 of a single cell. On the downside, they often consist of many equations and many  
246 parameters and their applicability on large ensembles of elements is highly ques-  
247 tionable, which also holds for a bifurcation analysis.

248 On the other side of the spectrum of complexity, there are normal-form equa-  
249 tions. These phenomenological models capture the main dynamical behavior of  
250 neurons such as the type of excitability and can be coupled together in large net-  
251 works with reasonable numerical effort. In some cases like the FitzHugh-Nagumo  
252 model [78, 79], they can be derived as low-dimensional approximations, which are  
253 better suited for a bifurcation analysis, because they contain only a few parameters  
254 and nonlinearities. The price that one has to pay is a vague - at best qualitative -

255 correspondence to physiological quantities like membrane potential, ionic currents,  
256 etc.

257 Self-organized dynamics of brain regions into functional networks often follow  
258 the underlying structural connections. There are, however, functional correlations  
259 between cortical regions that are not directly connected. Thus, the mechanisms  
260 for functional connectivity between distant cortical regions are still subject to  
261 intense research efforts. For example, indirect connections can support collective  
262 dynamical behavior on the brain network and pronounced pair-wise correlation  
263 of brain regions. If such indirect connections are involved, that is, there is no  
264 direct anatomical link between highly-correlated regions, the dynamical pattern  
265 can be called *remote synchronization* [80,82]. The amount of synchrony depends  
266 on properties of the coupling topology such as the symmetry of interactions [82,  
267 83].

### 268 3.2 The Kuramoto model of phase oscillators

269 Neural activity evolves through brain networks as a dynamical process, which can  
270 be approximated by either neural fields [84] or neural models [85]. To simulate the  
271 dynamical behavior of such processes, one can also choose the even simpler, that  
272 is less complex, model of Kuramoto-like phase oscillators [11–13,16], which has  
273 been established as a general model for oscillatory dynamics.

274 The classic Kuramoto model consists of dynamical equations with one phase  
275 variable for each network node [86]. The nodes are connected in an all-to-all topol-  
276 ogy and the interactions are mediated by sinusoidal functions of the phase differ-



277 ences of all pairs of oscillators:

$$\dot{\phi}_i = \omega_i + \frac{K}{N} \sum_{j=1}^N \sin[\phi_j(t) - \phi_i(t)], \quad i = 1, \dots, N, \quad (1)$$

278 where  $K$  is a global coupling strength. The parameter  $\omega_i$  denotes the natural  
 279 frequency of the  $i$ -th oscillator drawn from a given distribution. For reviews on the  
 280 relevance and universal applicability of the Kuramoto model see references [87,  
 281 88].

282 In order to analyze the amount of synchrony in the network, the global order  
 283 parameter, which is given by the center of mass of phase variables of each node  
 284 distributed on the unit circle, has proven to be very insightful:

$$R(t) = \left| \left\langle e^{i\phi_k(t)} \right\rangle_N \right|, \quad k = 1, \dots, N, \quad (2)$$

285 where  $\langle \cdot \rangle_N$  denotes the average over all nodes in the network. The order param-  
 286 eter can easily be applied to the simulated time series of neural activity [13, 89,  
 287 91]. Then, its temporal mean value  $\langle R(t) \rangle$  and standard deviation provide infor-  
 288 mation about the level and temporal fluctuations of synchrony. The latter can  
 289 be interpreted as metastability as discussed below. It is easy to see that in equa-  
 290 tion (2),  $R(t)$  tends to zero, if the phase variables are dispersed across phase space,  
 291 that is, when they are highly desynchronized. In the opposite case, when most of  
 292 oscillators have close phase variables, one obtains the limit  $R(t) \rightarrow 1$ .

293 In general, the number of phase variables that become locked and synchro-  
 294 nized, depends on the coupling strength  $K$ . This quantity can be used as a control  
 295 parameter to study emerging patterns of synchrony. For a given natural frequency  
 296 distribution, there is a threshold or critical coupling strength  $K_c$  above which the

297 coupled system starts to synchronize. This observation can be described as a phase  
 298 transition. Results based on the global order parameter defined in equation (2) can  
 299 be seen as a mean-field approach, that is, the simplest case of isotropic interaction.

300 To study neuro-biological systems, it is necessary to consider inhomogeneities  
 301 of the coupling topology connected to a variety of different complex networks.  
 302 In addition, one can investigate the influence of time delay in the coupling term.  
 303 Then, equation (1) can be extended as follows

$$\dot{\phi}_i = \omega_i + C \sum_{j=1}^N A_{ij} \sin[\phi_j(t - \tau_{ij}) - \phi_i(t)], \quad i = 1, \dots, N, \quad (3)$$

304 where the coupling strength is denoted by  $C$ . Now, structural inhomogeneities can  
 305 be accounted for by pair-wise transmission delays  $\tau_{ij}$  in the coupling term. This  
 306 makes network interactions biologically more plausible [92,81] and prevents full  
 307 synchronization of the network [82,93]. The delays are inferred from the distance  
 308  $\Delta_{ij}$  between nodes  $i$  and  $j$ :  $\tau_{ij} = \Delta_{ij}/v$  with a signal propagation velocity  $v$  in  
 309 the range of 1 m/s to 20 m/s. Alternatively, one can introduce link-dependent  
 310 phase offsets in the coupling term [94]. Less pronounced synchronization can be  
 311 interpreted as a preferred dynamical state and an important property of the neural  
 312 networks, as fully synchronized brain dynamics are never observed experimentally.  
 313 From the results of models of the resting-state dynamics, for instance, it has been  
 314 argued that the brain operates in so-called metastable states and never reaches  
 315 full synchronization [14,95].

316 The network matrix  $\{A_{ij}\}$  defines the interactions between the neural pro-  
 317 cesses. As elaborated in section 2, one can construct this matrix using empirically  
 318 derived structural connectivity: the non-zeros entries of the matrix correspond to

319 existing connections between respective brain regions. Alternatively, one could also  
320 generate an adjacency matrix based on the functional connectivity. Further details  
321 on the applied procedure, which uses a combination of anatomical and functional  
322 connectivity maps, will be discussed in section 4 below. See also figure 4.

### 323 3.3 Inferring BOLD signals: the Balloon-Windkessel model

324 As mentioned in section 2.1, functional connectivity maps are networks of brain  
325 regions that are based on a statistical dependence between fMRI time series [15,  
326 46,96]. The underlying time series of BOLD activity are a function of changes in  
327 cerebral blood flow, cerebral blood volume, and cerebral metabolic rate of oxygen  
328 consumption and typically exhibit significant correlations for frequencies below  
329 0.1 Hz in the resting state [46]. In order to compare the numerically obtained  
330 neuronal activity with the empirical BOLD signal, we make use of the Balloon-  
331 Windkessel model [97], which has been established in many computational studies  
332 of the resting-state brain activity. Briefly summarized, this model considers the  
333 neuronal time series as an input signal [98] and computes the hemodynamic re-  
334 sponse, which can then be related to the BOLD signal. Since the neuronal activity  
335 and the blood response operate on different time scales of milliseconds and sec-  
336 onds, respectively, the Balloon-Windkessel model acts as a low-pass filter on the  
337 high-frequency neuronal signal. To allow for comparison with the experimentally  
338 measured BOLD signal, we match a simulation's duration to the lengths of the  
339 experimental recording.

---

## 340 **4 Data-inspired models: from neuroimaging information to brain**

### 341 **activity models**

342 From a modeling perspective, the observed spatio-temporal patterns in brain ac-  
343 tivity are shaped by the complex relationship between the dynamics of individual  
344 oscillators and global synchronization [99]. As described in section 3.2, these com-  
345 peting dynamics can be characterized by the amount of synchrony in the network  
346 and its variations over time. The latter indicates dynamical metastability. It has  
347 been suggested that these variations of the network synchrony shape the patterns  
348 of coordinated activity between brain regions and thus, enabling dynamical ex-  
349 ploration of different network configurations [44,89,100]. Such functional network  
350 configurations are constrained by the underlying anatomical structure [101] – an-  
351 other key ingredient of the model.

352 Anatomical brain connections enter models of the brain dynamics in the form of  
353 the coupling matrix, whose elements represent actual neural paths between brain  
354 regions – network nodes – as described in section 2.1. The topology of this matrix  
355 is usually static, i.e., the number of links between the nodes is preserved. Figure 4  
356 provides a schematic diagram of the model workflow. A combination of experimen-  
357 tal anatomical and functional connectivity maps leads to an adjacency matrix that  
358 defines the interaction of the oscillators in the simulations. A link is present if it is  
359 anatomically justified and has a high probability to have functional connectivity,  
360 which is implemented as an element-wise multiplication of binarized anatomical  
361 and functional connectivity matrices. By averaging and binarizing the connectiv-  
362 ity matrices one can select the connections between pairs of regions with higher  
363 statistical probability, considering all subjects. Since the functional connectivity

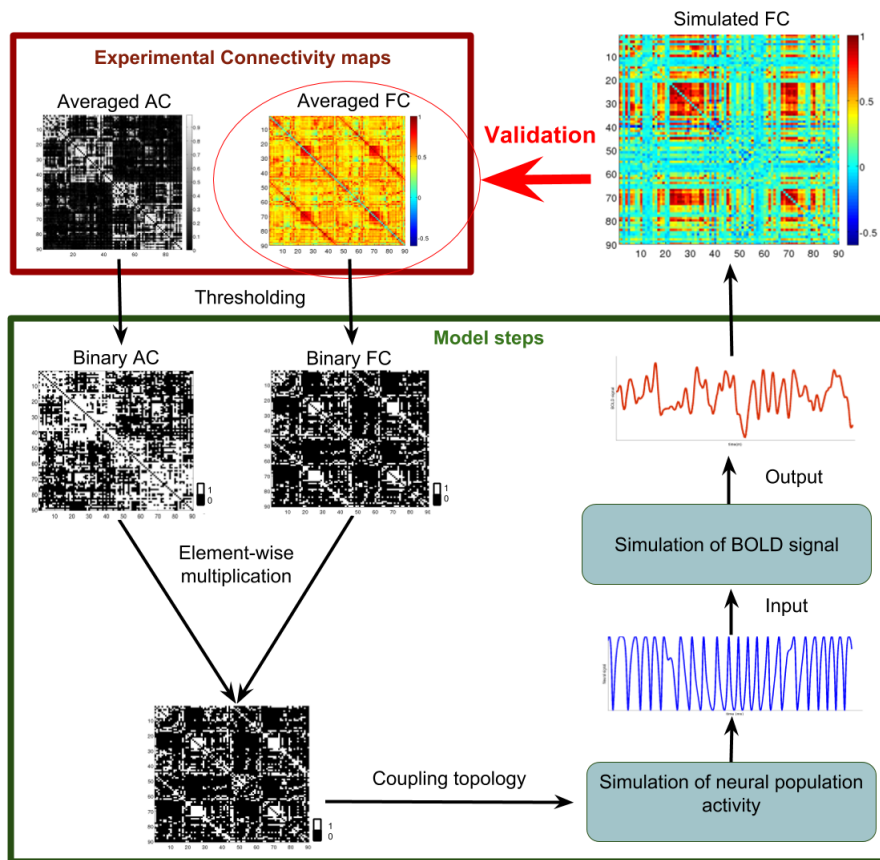


**Fig. 4** Schematic diagram for the modeling framework. Anatomical connectivity (AC) and functional connectivity (FC) maps extracted from DW-MRI and fMRI as group averages over 26 subjects, respectively, are binarized and combined to compute the adjacency matrix that provides the coupling topology in the simulations. Neural population activity is simulated and used as input to infer the simulated BOLD signal. The resulting time series of each node are correlated pair-wise leading to a simulated functional connectivity matrix, which is compared with the experimental functional connectivity map.

364 map has been derived from resting-state data, the element-wise multiplication se-  
 365 lects those anatomical connections that directly connect brain regions that tend to  
 366 be highly correlated in this condition. This step is important to evaluate the first  
 367 level influence of anatomical connections in the remote synchronization of brain  
 368 regions activities.

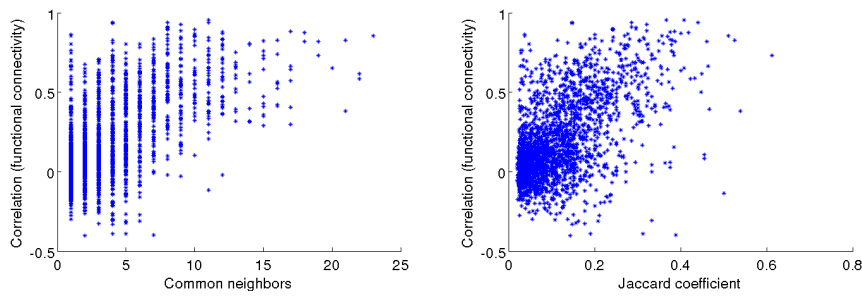


**Fig. 5** Functional connectivity between pairs of network nodes, i.e., regions of interest, which are not directly connected in the considered brain graph, as a function of the number of common neighbors (left) and Jaccard coefficient (right). Parameters in the simulation of equation (3) with delays calculated from the fiber lengths: threshold for functional connectivity in the network generation  $r = 0.56$ , coupling strength  $C = 54$ , and signal transmission velocity  $v = 5$  m/s.

369 We use this approach to derive the coupling topology for our simulations as our  
 370 primary aim is to reconstruct long-distance functional correlations that emerge  
 371 from the underlying anatomical paths. Previous works have used this model to  
 372 explore the contribution of the long-distance functional interactions – those that  
 373 are not supported by direct neural paths – to the brain functional correlations in  
 374 the resting-state activity [11,12]. These works have shown that the integration of  
 375 the brain functions may arise from relay-like phase interactions between neural  
 376 oscillators that share large parts of their individual network’s neighborhood. In  
 377 this review, we present additional analyses based on brain dynamics that include  
 378 time delays in the phase interactions between the neural oscillators, as given in  
 379 equation (3). The time-delayed interactions are determined by the empirical length  
 380 of the connections between the regions. See figure 2. It is worth mentioning that  
 381 the time delays on the real brain may be affected by heterogeneities related to  
 382 local physiology. For example, the velocity of signal transmission depends on other  
 383 biological aspects such as myelination and axon thickness. The model in this paper

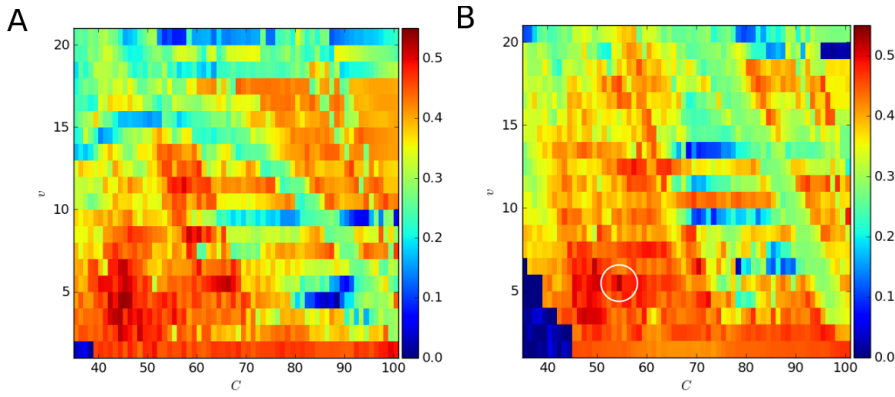


**Fig. 6** Pearson correlation coefficient between experimentally derived and simulated functional connectivity in the parameter space spanned by coupling strength  $C$  and signal transmission velocity  $v$ . The simulations are based on equation (3) with time delays calculated from the Euclidean distances and lengths of fiber tracks between regions of interest in panels A and B, respectively. See figure 2 for further information on the distances. The white circle in panel B marks the  $(C, v)$ -values used in figures 5 and 7 with a maximum Pearson correlation of 0.53.

384 accounts for the influence of time delay by (i) considering the heterogeneity of  
 385 distances and (ii) assuming a fixed velocity.

386 Figure 5 shows the effect of remote synchronization. It depicts the functional  
 387 connectivity for any pair of nodes  $i$  and  $j$  that do not share a direct connection ac-  
 388 cording to the coupling matrix in dependence on the number of common neighbors  
 389 and the relative overlap of the neighborhoods  $N_i$  and  $N_j$ . The latter is quantified  
 390 by the Jaccard coefficient

$$J_{ij} = \frac{|N_i \cap N_j|}{|N_i \cup N_j|}, \quad (4)$$

391 where  $|N_i|$  denotes the number of neighbors of node  $i$ , that is, its degree. In words,  
 392  $J_{ij}$  is the relative size of the intersection between the two node sets with respect  
 393 to their union and takes values in the interval  $[0, 1]$  with the limit cases of zero  
 394 and unity referring to no and perfect overlap, respectively. We observe an increase  
 395 of functional connectivity as the overlap of neighborhoods becomes larger. This is  
 396 in agreement with previous findings [11,12].

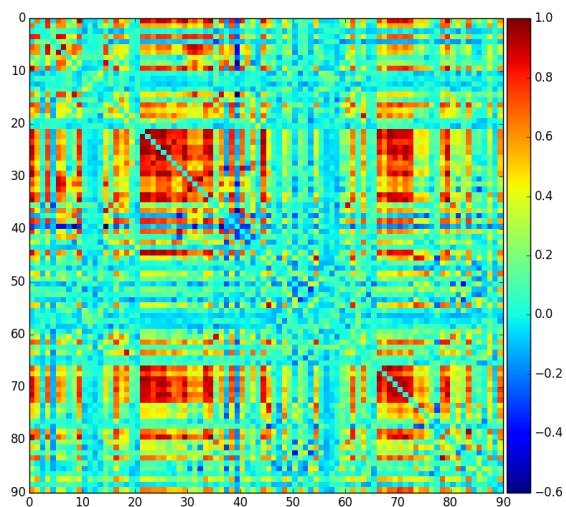


**Fig. 7** Exemplary, simulated functional connectivity based on equation (3) with time delays calculated from the fiber lengths between regions of interest (cf. figure 2). Parameters:  $C = 54$  and  $v = 5$  m/s.

397        A systematic exploration of the parameter space spanned by coupling strength  
398  $C$  and signal transmission velocity  $v$  is depicted in figure 6, where the left and right  
399 panels refer to time delays in equation (3) according to the Euclidean distances  
400 and lengths of fiber tracks between brain network nodes, respectively. Recall that  
401 the finite velocity is the cause of delayed interactions. The color code indicates  
402 the agreement with the experimentally derived and simulated functional connec-  
403 tivity quantified by the Pearson correlation coefficient. Overall, the results of the  
404 two panels in figure 6 are qualitatively very similar. Note that a rescaling in the  
405  $v$ -direction would lead to a quantitative agreement that could be explained by  
406 the shape of the distance distributions shown in figure 2. Larger velocities could  
407 compensate for the shorter distances. According to our analysis, the Euclidean dis-  
408 tance between different brain regions – with a proper scaling factor – can be used



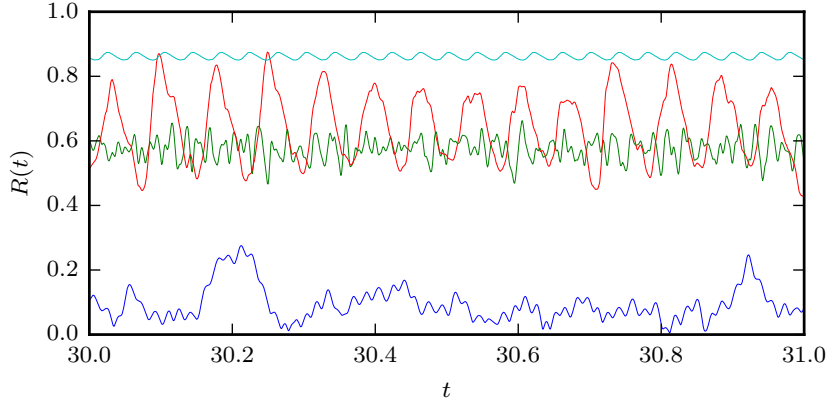


**Fig. 8** Global order parameter defined in equation (2) for different signal transmission velocities  $v = 0.1$  m/s (blue), 5 m/s (green), 20 m/s (red), and 100 m/s (cyan). The coupling strength is fixed at  $C = 54$ .

409 to account for finite signal transmission velocities along the neural connections.  
 410 The highest Pearson correlation is found in the range of plausible transmission  
 411 velocities. For weak coupling, that is, low values of  $C$ , the interaction via the net-  
 412 work is not strong enough to trigger significant self-organized synchrony in neural  
 413 activity or BOLD signals.

414 The best agreement of the simulated functional connectivity with the exper-  
 415 imental functional connectivity is observed for  $C = 54$  and  $v = 5$  m/s. Figure 7  
 416 shows the corresponding functional connectivity matrix obtained from the simu-  
 417 lations. One can see clusters of well-correlated nodes in the brain network.

418 Considering the form of the global order parameter  $R$  given by equation (2) the  
 419 particular parameter combination choice,  $C = 54$  and  $v = 5$  m/s, is justified. The  
 420 temporal average  $\langle R(t) \rangle$  of the order parameter quantifies the average amount  
 421 of synchrony in the brain network and its standard deviation can be used to  
 422 inspect metastability. Figure 8 depicts the time series of  $R$  for a fixed coupling  
 423 strength  $C = 54$  and different velocities  $v$ . Large values of  $v$  result in an almost

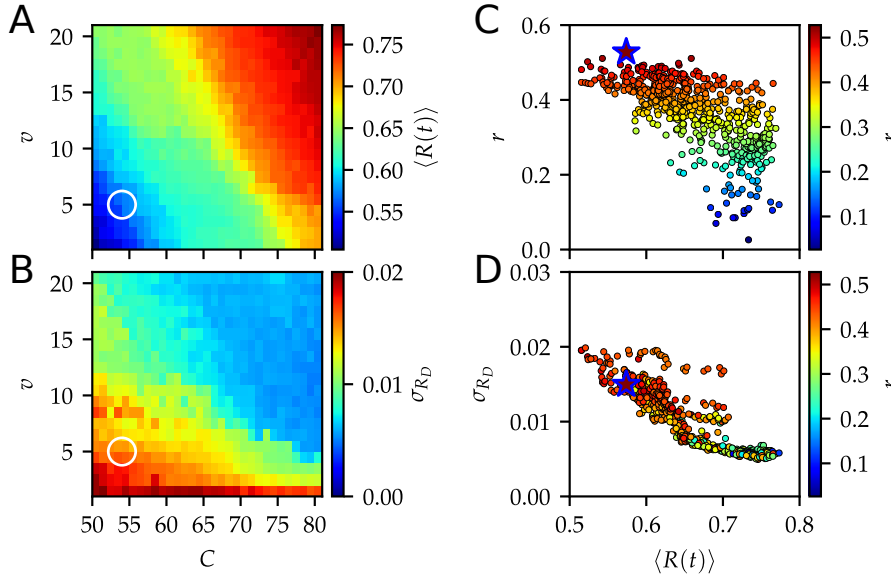


**Fig. 9** Panels A and B: parameter scan of the average order parameter  $\langle R \rangle$  and detrended fluctuations  $\sigma_{RD}$  as color code in the  $(C, v)$ -plane, respectively (cf. figure 6). Panels C and D: average order parameter  $\langle R \rangle$  vs. Pearson correlation and detrended fluctuations  $\sigma_{RD}$ , respectively. The color code refers to the Pearson correlation coefficient  $r$  between experimental and simulated functional connectivity (cf. figure. 6). The white circles and blue star marks the values  $C = 54$  and  $v = 5$  m/s used in figures 5 and 7 with a maximum Pearson correlation of 0.53. The fit of the modeled functional correlations with the experimental data is best for a dynamical state that simultaneously balances synchrony and metastability.

424 instantaneous coupling, for which the coupling function in equation (3) supports  
 425 the emergence of robust synchronization. This is indicated by a high value of  $R$  that  
 426 does not exhibit strong fluctuations around its mean (cyan curve,  $v = 100$  m/s).  
 427 As velocities decrease, the order parameter becomes smaller, but still remains its  
 428 periodicity (red curve,  $v = 20$  m/s). In the range of plausible velocities (cf. green  
 429 curve,  $v = 5$  m/s), we find a balance between synchrony and metastability, that is,  
 430 a reasonable value of  $\langle R(t) \rangle$  together with seemingly random fluctuations. These  
 431 observations are in agreement with our previous studies [11,12].

432 Figure 9 shows how functional interactions – high values of the correlation  
 433 coefficient  $r$  between the modeled and experimental dynamics – can be connected

434 to a dynamical behavior that balances the synchrony  $\langle R(t) \rangle$  and the variations  
435 in synchrony  $\sigma_{R_D}$ . Figures 9A and B depict the dependence of the average or-  
436 der parameter  $\langle R \rangle$  and its fluctuations  $\sigma_{R_D}$  on the coupling strength  $C$  and the  
437 transmission velocity  $v$ , respectively. For the fluctuations  $\sigma_{R_D}$ , we detrended the  
438 periodic behavior of  $R(t)$  (cf. figure 8). This detrending removes the contributions  
439 to the standard deviation that do not reflect fluctuations in the dynamics. One  
440 can see that the good agreement with the experimental matrix is found in a re-  
441 gion of the parameter space that presents some level of synchronization (panel A)  
442 and fluctuations (panel B). These dynamical conditions allow for the emergence of  
443 synchronization on the functional networks and also keep some level of flexibility  
444 for the emergence of different synchronized patterns over time. Figures 9C and D  
445 further corroborate this balance in the simulated, metastable dynamics. The val-  
446 ues  $C = 54$  and  $v = 5$  m/s, which lead the maximum Pearson correlation between  
447 simulated and experimental functional connectivities, are marked by white circles  
448 and a blue star. These findings are consistent with the previous simulations of  
449 task-free [13,44] and task-dependent [89] brain activity, which are based on sim-  
450 ilar simplified models that take into account a few key parameters of structural  
451 and functional brain connectivity.

452 The experimental fMRI data sets used in this paper are available from the *1000*  
453 *Functional Connectome Project* website ([http://fcon\\_1000.projects.nitrc.org/](http://fcon_1000.projects.nitrc.org/)).  
454 We consider functional scans from the Berlin Margulies data to calculate the group  
455 average. The data consist of open-eyes resting-state measurements of 26 subjects  
456 (ages: 23-44) [102]. For details on the pre-processing steps, see reference [11]. For  
457 the anatomical connectivity probability, we use DW-MRI data from a study de-  
458 scribed in reference [27].

## 459 **5 Conclusions**

460 Modern brain imaging methods allow for a quantitative study of both local activ-  
461 ity dynamics and the interdependence between activities in anatomically distant  
462 cortical areas, which is known as functional connectivity. With this review, we have  
463 summarized one of many multidisciplinary approaches to model such functional  
464 interactions. Leveraging interdisciplinary theoretical techniques, inspired by com-  
465 plex system theory and applied mathematics, and existing experimental data from  
466 noninvasive brain imaging, the proposed modeling framework contributes to the  
467 development of viable analytical and modeling techniques leading to significant  
468 insight into dynamical mechanisms of the brain.

469 The particular model, which we consider in this review, combines experimen-  
470 tal anatomical and functional connectivity between cortical regions to generate a  
471 network topology of the brain at rest. By varying the network interactions (using  
472 different coupling strengths and signal transmission velocities), it is possible to  
473 obtain correlation patterns in the simulated BOLD fMRI time series that are in  
474 agreement with experiments. We have shown that the model leads to the best  
475 agreement for a dynamical state that exhibits a balance between synchrony and  
476 temporal variations in synchrony. The proposed model allows to investigate the  
477 role of network structure and in particular indirect connections between distant  
478 cortical regions and to explore functional connectivity in the brain using numerical  
479 simulations of delay-coupled phase oscillators. For example, we have found higher  
480 functional connectivity, if the neighborhoods of respective nodes show a greater  
481 overlap. We have also compared the influence of time delay considering fiber track  
482 lengths and Euclidean distances between brain regions. We have observed no qual-

483 itative difference in the simulations. This means that Euclidean distances – after  
484 rescaling – may be used to account for realistic coupling delays.

485 The procedure can easily be extended to a much larger field of brain states.  
486 For example, one can alter the adjacency matrix of the task-negative system by  
487 increasing the weights of connections between task-related nodes above unity, sim-  
488 ulating a greater statistical relevance within the task-evoked state. Additionally,  
489 this procedure might give some insight into the brain shifting from the resting-state  
490 to task-evoked states and back.

491 The flexibility of the network topology generating process also gives an op-  
492 portunity to manipulate node connections to adapt to neural activity observed  
493 in fMRI measurements of patients suffering from various brain disorders. Indeed,  
494 similar data-driven models had contributed to understanding some mechanisms of  
495 brain disorders [103, 7, 90, 91].

496 The limitation of this model is given by its purpose, which was to provide expla-  
497 nations for mechanisms generating coordinated activity between spatially distant  
498 brain regions. We focus our computations on how these long-distance correlations  
499 arise from realistic functional interactions, i.e. those that are also supported by  
500 direct structural connections. Thus, our model does not consider the role of cou-  
501 pling topologies that correspond directly to structural connectivity data. Models  
502 based on these structural connectivity topologies have been explored extensively  
503 in several studies (see references [13, 89, 91]), reaching – similarly to our model –  
504 to an agreement with the experimental data only to a certain extent.

505 The model presented in this paper does not strive to give an accurate represen-  
506 tation of the physiologically realistic brain activity. A much more physiologically  
507 based approach is needed to achieve a full understanding of the relation between

508 experimental fMRI data and simulated neural activity. However, this goes beyond  
509 the scope of the main focus of the present work, that discusses a specific approach  
510 to find a simple way to simulate neural time series and to transform them into data,  
511 which can be compared to experimental fMRI measurements. This simplification  
512 is also adopted in similar studies found in references [13,44,91,95]. The model that  
513 we presented in this review can be extended in various way to incorporate more  
514 physiological details such as heterogeneities in the signal transmission velocities  
515 accounting for myelination or axon thickness. In addition, link weights can be in-  
516 troduced in the coupling matrix to include more information from experimental  
517 data.

518 The studies summarized in this article contribute to a better understanding of  
519 the relationship between complex brain networks and temporal dynamics of brain  
520 activity. They might also serve as a starting point to investigate brain network  
521 reconfigurations providing a modeling framework to explore transient, dynamical  
522 interactions, which enable diverse cognitive functions.

523 **Acknowledgements** AV and PH acknowledge support by Deutsche Forschungsgemeinschaft  
524 under grant no. HO4695/3-1 and within the framework of Collaborative Research Center 910.  
525 We thank Yasser Iturria-Medina for sharing the DW-MRI data including fiber lengths used in  
526 the study. We also thank Jason Bassett for helpful discussions.

## 527 **References**

- 528 1. T. Womelsdorf, J. M. Schoffelen, R. Oostenveld, W. Singer, and R. Desimone: *Modulation*  
529 *of neuronal interactions through neuronal synchronization*, Science **316**, 1609 (2007).
- 530 2. P. Uhlhaas, G. Pipa, B. Lima, L. Melloni, S. Neuenschwander, D. Nikolic, and W. Singer:  
531 *Neural synchrony in cortical networks: history, concept and current status*, Front. Integr.

- 532 Neurosci. **3**, 17 (2009).
- 533 3. M. Bola and B. A. Sabel: *Dynamic reorganization of brain functional networks during*  
534 *cognition*, NeuroImage **114**, 398 (2015).
- 535 4. C. J. Honey, O. Sporns, L. Cammoun, X. Gigandet, J. P. Thiran, R. Meuli, and P. Hag-  
536 mann: *Predicting human resting-state functional connectivity from structural connectiv-*  
537 *ity*, Proc. Natl. Acad. Sci. U.S.A. **106**, 2035 (2009).
- 538 5. G. Deco, V. K. Jirsa, and A. R. McIntosh: *Emerging concepts for the dynamical organi-*  
539 *zation of resting-state activity in the brain.*, Nat. Rev. Neurosci. **12**, 43 (2011).
- 540 6. S. F. Muldoon, F. Pasqualetti, S. Gu, M. Cieslak, S. T. Grafton, J. M. Vettel, and D. S.  
541 Bassett: *Stimulation-based control of dynamic brain networks*, PLoS Comput. Biol. **12**,  
542 e1005076 (2016).
- 543 7. F. Hutchings, C. E. Han, S. S. Keller, B. Weber, P. N. Taylor, and M. Kaiser: *Predicting*  
544 *surgery targets in temporal lobe epilepsy through structural connectome based simula-*  
545 *tions*, PLoS Comput. Biol. **11**, e1004642 (2015).
- 546 8. P. Sanz-Leon, S. A. Knock, A. Spiegler, and V. K. Jirsa: *Mathematical framework for*  
547 *large-scale brain network modeling in The Virtual Brain*, Neuroimage **111**, 385 (2015).
- 548 9. S. H. Strogatz: *From Kuramoto to Crawford: exploring the onset of synchronization in*  
549 *populations of coupled oscillators*, Physica D **143**, 1 (2000).
- 550 10. V. Vuksanović and P. Hövel: *Large-scale neural network model for functional networks of*  
551 *the human cortex*, in *Selforganization in Complex Systems: The Past, Present, and Fu-*  
552 *ture of Synergetics, Proc. of the International Symposium, Hanse Institute of Advanced*  
553 *Studies Delmenhorst*, edited by A. Pelster and G. Wunner (Springer, Berlin, 2016), Un-  
554 derstanding Complex Systems, pp. 345–352.
- 555 11. V. Vuksanović and P. Hövel: *Functional connectivity of distant cortical regions: Role of*  
556 *remote synchronization and symmetry in interactions*, NeuroImage **97**, 1 (2014).
- 557 12. V. Vuksanović and P. Hövel: *Dynamic changes in network synchrony reveal resting-state*  
558 *functional networks*, Chaos **25**, 023116 (2015).
- 559 13. J. Cabral, E. Hugues, O. Sporns, and G. Deco: *Role of local network oscillations in*  
560 *resting-state functional connectivity*, Neuroimage **57**, 130 (2011).
- 561 14. J. Cabral, H. Luckhoo, M. W. Woolrich, M. Joensuu, H. Mohseni, A. Baker, M. L.  
562 Kringelbach, and G. Deco: *Exploring mechanisms of spontaneous functional connectivity*

- 563        *in MEG: How delayed network interactions lead to structured amplitude envelopes of*  
564        *band-pass filtered oscillations*, *Neuroimage* **90**, 423 (2014).
- 565 15. S. L. Bressler and V. Menon: *Large-scale brain networks in cognition: emerging methods*  
566        *and principles*, *Trends Cogn. Sci.* **14**, 277 (2010).
- 567 16. M. Breakspear, S. Heitmann, and A. Daffertshofer: *Generative models of cortical oscil-*  
568        *lations: neurobiological implications of the Kuramoto model*, *Front. Hum. Neurosci.* **4**,  
569        190 (2010).
- 570 17. M. Wildie and M. Shanahan: *Hierarchical clustering identifies hub nodes in a model of*  
571        *resting-state brain activity*, in *Neural Networks (IJCNN), The 2012 International Joint*  
572        *Conference on* (IEEE, 2012), pp. 1–6.
- 573 18. F. Vása, M. Shanahan, P. J. Hellyer, G. Scott, J. Cabral, and R. Leech: *Effects of lesions*  
574        *on synchrony and metastability in cortical networks*, *NeuroImage* **118**, 456 (2015).
- 575 19. J. Cabral, H. M. Fernandes, T. J. Van Hartevelt, A. C. James, and M. L. Kringelbach:  
576        *Structural connectivity in schizophrenia and its impact on the dynamics of spontaneous*  
577        *functional networks*, *Chaos* **23**, 046111 (2013).
- 578 20. M. Shanahan: *Metastable chimera states in community-structured oscillator networks*,  
579        *Chaos* **20**, 013108 (2010).
- 580 21. N. Kanwisher: *Functional specificity in the human brain: a window into the functional*  
581        *architecture of the mind*, *Proc. Natl. Acad. Sci. U.S.A.* **107**, 11163 (2010).
- 582 22. J. D. Schall: *On Building a Bridge Between Brain and Behavior*, *Annu. Rev. Psych.* **55**,  
583        23 (2004).
- 584 23. O. Sporns: *Structure and function of complex brain networks*, *Dialogues Clin. Neurosci.*  
585        **15**, 247 (2013).
- 586 24. J. D. Haynes and G. Rees: *Decoding mental states from brain activity in humans*, *Nat.*  
587        *Rev. Neurosci.* **7**, 523 (2006).
- 588 25. H. Farooq, J. Xu, J. W. Nam, D. F. Keefe, E. Yacoub, T. Georgiou, and C. Lenglet:  
589        *Microstructure imaging of crossing (MIX) white matter fibers from diffusion MRI*, *Sci.*  
590        *Rep.* **6**, 38927 (2016).
- 591 26. M. Xia, J. Wang, and Y. He: *Brainnet viewer: A network visualization tool for human*  
592        *brain connectomics*, *PLoS ONE* **8**, 1 (2013).



- 593 27. Y. Iturria-Medina, R. C. Sotero, E. J. Canales-Rodríguez, Y. Alemán-Gómez, and  
594 L. Melie-García: *Studying the human brain anatomical network via diffusion-weighted*  
595 *MRI and graph theory*, NeuroImage **40**, 1064 (2008).
- 596 28. O. Sporns, G. Tononi, and R. Kötter: *The human connectome: a structural description*  
597 *of the human brain*, PLoS Comput. Biol. **1**, e42 (2005).
- 598 29. D. J. Felleman and D. C. Van Essen: *Distributed hierarchical processing in the primate*  
599 *cerebral cortex*, Cerebral Cortex **1**, 1 (1991).
- 600 30. O. Ciccarelli, M. Catani, H. Johansen-Berg, C. Clark, and A. Thompson: *Diffusion-based*  
601 *tractography in neurological disorders: concepts, applications, and future developments*,  
602 Lancet Neurol. **7**, 715 (2008).
- 603 31. J. D. Clayden: *Imaging connectivity: MRI and the structural networks of the brain*,  
604 Funct. Neurol. **28**, 197 (2013).
- 605 32. S. Jbabdi, S. N. Sotiropoulos, S. N. Haber, D. C. Van Essen, and T. E. Behrens: *Measuring*  
606 *macroscopic brain connections in vivo*, Nat. Neurosci. **18**, 1546 (2015).
- 607 33. N. Tzourio-Mazoyer, B. Landeau, D. Papathanassiou, F. Crivello, O. Etard, N. Delcroix,  
608 B. Mazoyer, and M. Joliot: *Automated anatomical labeling of activations in SPM using a*  
609 *macroscopic anatomical parcellation of the MNI MRI single-subject brain*, Neuroimage  
610 **15**, 273 (2002).
- 611 34. D. J. Heeger and D. Ress: *What does MRI tell us about neuronal activity?*, Nat. Rev.  
612 Neurosci. **3**, 142 (2002).
- 613 35. J. Talairach and P. Tournoux: *Co-planar stereotaxic atlas of the human brain. 3-*  
614 *Dimensional proportional system: an approach to cerebral imaging* (Thieme, New York,  
615 1988).
- 616 36. D. N. Greve, G. G. Brown, B. A. Mueller, G. Glover, and T. T. Liu: *A survey of the*  
617 *sources of noise in fmri*, Psychometrika **78**, 396 (2013).
- 618 37. J. D. Power, A. Mitra, T. O. Laumann, A. Z. Snyder, B. L. Schlaggar, and S. E. Petersen:  
619 *Methods to detect, characterize, and remove motion artifact in resting state fMRI*, Neu-  
620 roimage **84**, 320 (2014).
- 621 38. F. Kruggel, D. Y. von Cramon, and X. Descombes: *Comparison of filtering methods for*  
622 *fMRI datasets*, NeuroImage **10**, 530 (1999).

- 623 39. A. E. Desjardins, K. A. Kiehl, and P. F. Liddle: *Removal of confounding effects of global*  
624 *signal in functional MRI analyses*, NeuroImage **13**, 751 (2001).
- 625 40. M. Rubinov and O. Sporns: *Complex network measures of brain connectivity: uses and*  
626 *interpretations.*, Neuroimage **52**, 1059 (2010).
- 627 41. E. T. Bullmore and D. S. Bassett: *Brain graphs: graphical models of the human brain*  
628 *connectome*, Annu. Rev. Clin. Psychol. **7**, 113 (2011).
- 629 42. Y. Liu, M. Liang, Y. Zhou, Y. He, Y. Hao, M. Song, C. Yu, H. Liu, Z. Liu, and T. Jiang:  
630 *Disrupted small-world networks in schizophrenia*, Brain **131**, 945 (2008).
- 631 43. H. Onias, A. Viol, F. Palhano-Fontes, K. C. Andrade, M. Sturzbecher, G. M.  
632 Viswanathan, and D. B. de Araujo: *Brain complex network analysis by means of rest-*  
633 *ing state fMRI and graph analysis: Will it be helpful in clinical epilepsy?*, Epilepsy &  
634 Behavior **38**, 71 (2014).
- 635 44. J. Cabral, M. L. Kringelbach, and G. Deco: *Exploring the network dynamics underlying*  
636 *brain activity during rest*, Prog. Neurobiol. **114**, 102 (2014).
- 637 45. O. Sporns: *Networks of the brain* (MIT Press, Cambridge, MA, USA, 2011).
- 638 46. B. Biswal, F. Z. Yetkin, V. M. Haughton, and J. S. Hyde: *Functional connectivity in the*  
639 *motor cortex of resting human brain using echo-planar MRI*, Magn. Reson. Med. **34**,  
640 537 (1995).
- 641 47. M. J. Lowe: *A historical perspective on the evolution of resting-state functional connec-*  
642 *tivity with MRI*, Magn. Reson. Mater. Phys. **23**, 279 (2010).
- 643 48. D. M. Cole, S. M. Smith, and C. F. Beckmann: *Advances and pitfalls in the analysis and*  
644 *interpretation of resting-state FMRI data*, Front. Syst. Neurosci. **4**, 8 (2010).
- 645 49. M. P. van den Heuvel and H. E. Hulshoff Pol: *Exploring the brain network: A review on*  
646 *resting-state fMRI functional connectivity*, Eur. Neuropsychopharmacol. **20**, 519 (2010).
- 647 50. E. Tagliazucchi, R. Carhart-Harris, R. Leech, D. Nutt, and D. R. Chialvo: *Enhanced*  
648 *repertoire of brain dynamical states during the psychedelic experience*, Hum. Brain Mapp.  
649 **35**, 5442 (2014).
- 650 51. R. Carhart-Harris, S. Muthukumaraswamy, L. Roseman, M. Kaelen, W. Droog, K. Mur-  
651 phy, E. Tagliazucchi, E. E. Schenber, T. Nest, C. Orban, R. Leech, L. T. Williams, T. M.  
652 Williams, M. Bolstridge, B. Sessa, J. McGonigle, M. I. Sereno, D. Nichols, P. J. Hellyer,  
653 P. Hobden, J. Evans, K. D. Singh, R. G. Wise, H. V. Curran, A. Feilding, and D. J.

- 654 Nutt: *Neural correlates of the LSD experience revealed by multimodal neuroimaging*,  
655 Proc. Natl. Acad. Sci. U.S.A. **113**, 4853 (2016).
- 656 52. A. Viol, F. Palhano-Fontes, H. Onias, D. B. de Araujo, and G. M. Viswanathan: *Shan-*  
657 *non entropy of brain functional complex networks under the influence of the psychedelic*  
658 *Ayahuasca*, Sci. Rep. **7**, 7388 (2017).
- 659 53. J. D. Rudie, J. A. Brown, D. Beck-Pancer, L. M. Hernandez, E. L. Dennis, P. M. Thomp-  
660 son, S. Y. Bookheimer, and M. Dapretto: *Altered functional and structural brain network*  
661 *organization in autism*, NeuroImage: Clinical **2**, 79 (2013).
- 662 54. M. Rubinov, S. A. Knock, C. J. Stam, S. Micheloyannis, A. W. F. Harris, L. M. Williams,  
663 and M. Breakspear: *Small-world properties of nonlinear brain activity in schizophrenia*,  
664 Hum. Brain Mapp. **30**, 403 (2009).
- 665 55. J. Schrouff, V. Perlbarg, M. Boly, G. Marrelec, P. Boveroux, A. Vanhaudenhuyse, M. A.  
666 Bruno, S. Laureys, C. Phillips, M. Péligrini-Issac, P. Maquet, and H. Benali: *Brain func-*  
667 *tional integration decreases during propofol-induced loss of consciousness*, NeuroImage  
668 **57**, 198 (2011).
- 669 56. T. T. Dang-Vu, M. Schabus, M. Desseilles, G. Albouy, M. Boly, A. Darsaud, S. Gais,  
670 G. Rauchs, V. Sterpenich, G. Vandewalle, J. Carrier, G. Moonen, E. Balteau, C. Deguel-  
671 dre, A. Luxen, C. Phillips, and P. Maquet: *Spontaneous neural activity during human*  
672 *slow wave sleep*, Proc. Natl. Acad. Sci. U.S.A. **105**, 15160 (2008).
- 673 57. Q. Noirhomme, A. Soddu, R. Lehenbre, A. Vanhaudenhuyse, P. Boveroux, M. Boly, and  
674 S. Laureys: *Brain connectivity in pathological and pharmacological coma*, Front. Syst.  
675 Neurosci. **4**, 160 (2010).
- 676 58. Z. Huang, R. Dai, X. Wu, Z. Yang, D. Liu, J. Hu, L. Gao, W. Tang, Y. Mao, Y. Jin,  
677 X. Wu, B. Liu, Y. Zhang, L. Lu, S. Laureys, X. Weng, and G. Northoff: *The self and*  
678 *its resting state in consciousness: An investigation of the vegetative state*, Hum. Brain  
679 Mapp. **35**, 1997 (2014).
- 680 59. P. Barttfeld, L. Uhrig, J. D. Sitt, M. Sigman, B. Jarraya, and S. Dehaene: *Signature*  
681 *of consciousness in the dynamics of resting-state brain activity*, Proc. Natl. Acad. Sci.  
682 U.S.A. **112**, 887 (2015).
- 683 60. G. Deco, V. K. Jirsa, and A. R. McIntosh: *Resting brains never rest: computational*  
684 *insights into potential cognitive architectures*, Trends Neurosci. **36**, 268 (2013).

- 685 61. M. A. Koch, D. G. Norris, and M. Hund-Georgiadis: *An Investigation of Functional*  
686 *and Anatomical Connectivity Using Magnetic Resonance Imaging*, *NeuroImage* **16**, 241  
687 (2002).
- 688 62. A. Pikovsky, M. G. Rosenblum, and J. Kurths: *Synchronization: a universal concept in*  
689 *nonlinear sciences* (Cambridge University Press, Cambridge, 2001).
- 690 63. S. Boccaletti, J. Kurths, G. Osipov, D. L. Valladares, and C. S. Zhou: *The synchronization*  
691 *of chaotic systems*, *Phys. Rep.* **366**, 1 (2002).
- 692 64. E. Mosekilde, Y. Maistrenko, and D. Postnov: *Chaotic Synchronization: Applications to*  
693 *Living Systems* (World Scientific, Singapore, 2002).
- 694 65. A. G. Balanov, N. B. Janson, D. E. Postnov, and O. V. Sosnovtseva: *Synchronization:*  
695 *From Simple to Complex* (Springer, Berlin, 2009).
- 696 66. E. Rossoni, Y. Chen, M. Ding, and J. Feng: *Stability of synchronous oscillations in a*  
697 *system of Hodgkin-Huxley neurons with delayed diffusive and pulsed coupling*, *Phys. Rev.*  
698 *E* **71**, 061904 (2005).
- 699 67. Q. Y. Wang and Q. S. Lu: *Time delay-enhanced synchronization and regularization in*  
700 *two coupled chaotic neurons*, *Chin. Phys. Lett.* **22**, 543 (2005).
- 701 68. C. Hauptmann, O. E. Omel'chenko, O. Popovych, Y. Maistrenko, and P. Tass: *Control of*  
702 *spatially patterned synchrony with multisite delayed feedback*, *Phys. Rev. E* **76**, 066209  
703 (2007).
- 704 69. C. Masoller, M. C. Torrent, and J. García-Ojalvo: *Interplay of subthreshold activity,*  
705 *time-delayed feedback, and noise on neuronal firing patterns*, *Phys. Rev. E* **78**, 041907  
706 (2008).
- 707 70. Q. Wang, Q. Lu, and G. Chen: *Synchronization transition induced by synaptic delay in*  
708 *coupled fast-spiking neurons*, *Int. J. Bifur. Chaos* **18**, 1189 (2008).
- 709 71. Q. Wang, Q. Lu, G. Chen, Z. Feng, and L. X. Duan: *Bifurcation and synchronization of*  
710 *synaptically coupled FHN models with time delay*, *Chaos, Solitons and Fractals* **39**, 918  
711 (2009).
- 712 72. C. Masoller, M. C. Torrent, and J. García-Ojalvo: *Dynamics of globally delay-coupled*  
713 *neurons displaying subthreshold oscillations*, *Philosophical Transactions of the Royal*  
714 *Society A: Mathematical, Physical and Engineering Sciences* **367**, 3255 (2009).

- 715 73. D. V. Senthilkumar, J. Kurths, and M. Lakshmanan: *Inverse synchronizations in coupled*  
716 *time-delay systems with inhibitory coupling*, Chaos **19**, 023107 (2009).
- 717 74. X. Liang, M. Tang, M. Dhamala, and Z. Liu: *Phase synchronization of inhibitory bursting*  
718 *neurons induced by distributed time delays in chemical coupling*, Phys. Rev. E **80**, 066202  
719 (2009).
- 720 75. J. Lehnert, T. Dahms, P. Hövel, and E. Schöll: *Loss of synchronization in complex neural*  
721 *networks with delay*, Europhys. Lett. **96**, 60013 (2011).
- 722 76. O. Popovych, S. Yanchuk, and P. Tass: *Delay- and coupling-induced firing patterns in*  
723 *oscillatory neural loops*, Phys. Rev. Lett. **107**, 228102 (2011).
- 724 77. A. L. Hodgkin and A. F. Huxley: *A quantitative description of membrane current and*  
725 *its application to conduction and excitation in nerve*, J. Physiol. **117**, 500 (1952).
- 726 78. R. FitzHugh: *Impulses and physiological states in theoretical models of nerve membrane*,  
727 Biophys. J. **1**, 445 (1961).
- 728 79. J. Nagumo, S. Arimoto, and S. Yoshizawa.: *An active pulse transmission line simulating*  
729 *nerve axon.*, Proc. IRE **50**, 2061 (1962).
- 730 80. A. Bergner, M. Frasca, G. Sciuto, A. Buscarino, E. J. Ngamga, L. Fortuna, and J. Kurths:  
731 *Remote synchronization in star networks*, Phys. Rev. E **85**, 026208 (2012).
- 732 81. M. Breakspear, J. A. Roberts, J. R. Terry, S. Rodrigues, N. Mahant, and P. A. Robinson:  
733 *A unifying explanation of primary generalized seizures through nonlinear brain modeling*  
734 *and bifurcation analysis*, Cereb. Cortex **16**, 1296 (2006).
- 735 82. V. Nicosia, M. Valencia, M. Chavez, A. Díaz-Guilera, and V. Latora: *Remote synchroniza-*  
736 *tion reveals network symmetries and functional modules*, Phys. Rev. Lett. **110**, 174102  
737 (2013).
- 738 83. A. Arenas, A. Díaz-Guilera, and C. J. Pérez Vicente: *Synchronization reveals topological*  
739 *scales in complex networks*, Phys. Rev. Lett. **96**, 114102 (2006).
- 740 84. V. K. Jirsa and H. Haken: *Field theory of electromagnetic brain activity*, Phys. Rev. Lett.  
741 **77**, 960 (1996).
- 742 85. E. M. Izhikevich: *Which model to use for cortical spiking neurons?*, IEEE Transactions  
743 on Neural Networks **15**, 1063 (2004).

- 744 86. Y. Kuramoto: *Self-entrainment of a population of coupled non-linear oscillators*, in *Inter-*  
745 *national symposium on mathematical problems in theoretical physics*, edited by H. Araki  
746 (Springer, 1975), vol. 39 of *Lecture Notes in Physics*, pp. 420–422.
- 747 87. J. A. Acebrón, L. L. Bonilla, C. J. Pérez Vicente, F. Ritort, and R. Spigler: *The Kuramoto*  
748 *model: A simple paradigm for synchronization phenomena*, *Rev. Mod. Phys.* **77**, 137  
749 (2005).
- 750 88. F. A. Rodrigues, T. K. D. M. Peron, P. Ji, and J. Kurths: *The Kuramoto model in*  
751 *complex networks*, *Phys. Rep.* **610**, 1 (2016).
- 752 89. P. J. Hellyer, M. Shanahan, G. Scott, R. J. S. Wise, D. J. Sharp, and R. Leech: *The*  
753 *control of global brain dynamics: Opposing actions of frontoparietal control and default*  
754 *mode networks on attention*, *J. Neurosci.* **34**, 451 (2014).
- 755 90. G. Deco and M. L. Kringelbach: *Great expectations: Using whole-brain computational*  
756 *connectomics for understanding neuropsychiatric disorders*, *Neuron* **84**, 892 (2014).
- 757 91. J. Cabral, E. Hugues, M. L. Kringelbach, and G. Deco: *Modeling the outcome of structural*  
758 *disconnection on resting-state functional connectivity*, *Neuroimage* **62**, 1342 (2012).
- 759 92. M. Breakspear, S. Heitmann, and A. Daffertshofer: *Generative models of cortical oscil-*  
760 *lations: neurobiological implications of the Kuramoto model*, *Front. Hum. Neurosci.* **4**,  
761 190 (2010).
- 762 93. A. Keane, T. Dahms, J. Lehnert, S. A. Suryanarayana, P. Hövel, and E. Schöll: *Synchro-*  
763 *nisation in networks of delay-coupled type-I excitable systems*, *Eur. Phys. J. B* **85**, 407  
764 (2012).
- 765 94. V. Vuksanović and P. Hövel: *Role of structural inhomogeneities in resting-state brain*  
766 *dynamics*, *Cogn. Neurodyn.* **10**, 361 (2016).
- 767 95. G. Deco and V. K. Jirsa: *Ongoing cortical activity at rest: criticality, multistability, and*  
768 *ghost attractors*, *J. Neurosci.* **32**, 3366 (2012).
- 769 96. J. S. Damoiseaux, S. A. R. B. Rombouts, F. Barkhof, P. Scheltens, C. J. Stam, S. M.  
770 Smith, and C. F. Beckmann: *Consistent resting-state networks across healthy subjects*,  
771 *Proc. Natl. Acad. Sci. U.S.A.* **103**, 13848 (2006).
- 772 97. K. Friston, A. Mechelli, R. Turner, and C. J. Price: *Nonlinear responses in fMRI: The*  
773 *balloon model, Volterra kernels, and other hemodynamics*, *NeuroImage* **12**, 466 (2000).

- 
- 774 98. A. K. Seth, P. Chorley, and L. C. Barnett: *Granger causality analysis of fMRI BOLD*  
775 *signals is invariant to hemodynamic convolution but not downsampling*, *NeuroImage* **65**,  
776 540 (2013).
- 777 99. K. Friston and R. J. Dolan: *Computational and dynamic models in neuroimaging*, *Neu-*  
778 *roImage* **52**, 752 (2010).
- 779 100. E. Tognoli and J. A. S. Kelso: *The metastable brain*, *Neuron* **81**, 35 (2014).
- 780 101. E. T. Bullmore and O. Sporns: *Complex brain networks: graph theoretical analysis of*  
781 *structural and functional systems*, *Nat. Rev. Neurosci.* **10**, 186 (2009).
- 782 102. B. B. Biswal: *Toward discovery science of human brain function*, *Proc. Natl. Acad. Sci.*  
783 *U.S.A.* **107**, 4734 (2010).
- 784 103. M. Demirtas and G. Deco: *Chapter 4 - computational models of dysconnectivity in large-*  
785 *scale resting-state networks*, in *Computational Psychiatry*, edited by A. Anticevic and  
786 J. D. Murray (Academic Press, 2018), pp. 87–116.

787 **A List of cortical and sub-cortical regions**

**Table 1** Cortical and sub-cortical regions according to the automated anatomic labelling (AAL) template image [33]. Indexes from 1-45 and 46-90 indicate right (R) and left (L) hemisphere respectively, and refer to the order in which the brain regions of interest are arranged in all connectivity, adjacency and distance matrices of this paper.

Index R/L	Anatomical Description	Label
1/46	Precentral	PRE
2/47	Frontal Sup	F1
3/48	Frontal Sup Orb	F10
4/49	Frontal Mid	F2
5/50	Frontal Mid Orb	F20
6/51	Frontal Inf Oper	F30P
7/52	Frontal Inf Tri	F3T
8/53	Frontal Inf Orb	F30
9/54	Rolandic Oper	RO
10/55	Supp Motor Area	SMA
11/56	Olfactory	OC
12/57	Frontal Sup Medial	F1M
13/58	Frontal Mid Orb	SMG
14/59	Gyrus Rectus	GR
15/60	Insula	IN
16/61	Cingulum Ant	ACIN
17/62	Cingulum Mid	MCIN
18/63	Cingulum Post	PCIN
19/64	Hippocampus	HIP
20/65	ParaHippocampal	PHIP
21/66	Amygdala	AMYG
22/67	Calcarine	V1
23/68	Cuneus	Q
24/69	Lingual	LING
25/70	Occipital Sup	O1
26/71	Occipital Mid	O2
27/72	Occipital Inf	O3
28/73	Fusiform	FUSI
29/74	Postcentral	POST
30/75	Parietal Sup	P1
31/76	Parietal Inf	P2
32/77	Supra Marginal Gyrus	SMG
33/78	Angular	AG
34/79	Precuneus	PQ
35/80	Paracentral Lobule	PCL
36/81	Caudate	CAM
37/82	Putamen	PUT
38/83	Pallidum	PAL
39/84	Thalamus	THA
40/85	Heschi	HES
41/86	Temporal Sup	T1
42/87	Temporal Pole sup	T1P
43/88	Temporal Mid	T2
44/89	Temporal Pole Mid	T2P
45/90	Temporal Inf	T3